EPSC Abstracts
Vol. 10, EPSC2015-10, 2015
European Planetary Science Congress 2015

Wavelet-Based Multifractal Analysis of Demeter satellite data before the L'Aquila earthquake

S. Ouadfeul (1), V. Tourtchine (1) and L. Aliouanen (2)
(1) LIMOSE, Faculté des Sciences, Université Mhamed Bougara de Boumèrdes, Boumèrdes, Algeria, (2) LABOPHYT, Faculté des Hydrocarbures et de la Chimie, Université Mhamed Bougara de Boumèrdes, Boumèrdes, Algeria. (SOuadfeul@ymail.com)

Abstract

The main goal of this paper is to demonstrate the multifractal behavior of the ionospheric plasma signals recorded by the ISL instrument installed in the Demeter satellite before the L'Aquila earthquake. Multifractal analysis is performed using the so-called the Wavelet Transform Modulus Maxima lines (WTMM) method. Signals to be analyzed are: the electrons and ions densities, electrons temperature and the plasma potential. WTMM analysis of the data recorded during the 04th of April 2009 which recognizes many ionospheric disturbances before the L'Aquila earthquake clearly shows the multifractal behavior of the ionosphere plasma physical response.
Keywords: Multifractal, WTMM, ISL, Demeter, L'Aquila earthquake.

EPSC Abstracts
Vol. 10, EPSC2015-26, 2015
European Planetary Science Congress 2015

The effects of IMF sector boundary crossings on the induced magnetosphere of Venus

D. Vech (1,2), G. Stenberg (2) , H. Nilsson (2), N. J. T. Edberg (3), A. Opitz (4), K. Szegő (4), T. L. Zhang (5), Y. Futaana (2)
(1) Luleå University of Technology, Kiruna, Sweden (2) Swedish Institute of Space Physics, Kiruna, Sweden, (3) Swedish Institute of Space Physics, Uppsala, Sweden, (4) Wigner Research Centre for Physics, Budapest, Hungary, (5) Space Research Institute, Austrian Academy of Sciences, Graz, Austria (vech.daniel@wigner.mta.hu)

Abstract

The induced planetary magnetosphere is the result of the interaction between the streaming solar wind plasma and an unmagnetized planetary body with an ionosphere acting as an obstacle. The structure of the induced magnetosphere highly depends on the upstream solar wind parameters including the direction and magnitude of the Interplanetary Magnetic Field (IMF). (e.g. *Zhang et al.*, 2009; *Masunaga et al.*, 2011).

Not only the upstream conditions but also temporal variations of the upstream conditions are expected to cause changes in the structure of induced magnetospheres. For example, *Niedner and Brandt* [1978] reported that the cometary ion tail was lost due to reconnection after an IMF sector boundary crossing. *Edberg et al.* [2011] studied the effects of Interplanetary Coronal Mass Ejections (ICME) and Co-rotating Interaction Regions (CIR) at Venus. They suggested that the change in the magnetic field polarity during IMF sector boundary crossings contribute to an increased ion outflow. In addition, they speculated that this might be due to dayside magnetic reconnection.

In this study we aim to understand the effects of the varying upstream conditions on the Venusian induced magnetosphere. Using the entire Venus Express/ASPERA-4 and MAG datasets, we first produce the spatial distribution of ions in the plasma environment of Venus during ICME and CIR passages together with that during the average condition. In addition to ICME/CIR passages, we focus on the Heliospheric Current Sheet (HCS) crossings, which can also change the polarity of the induced magnetosphere. By comparing HCS events and ICME/CIR events, we may be able to distinguish the contribution of IMF polarity change on the Venusian induced magnetosphere, because the solar wind is less disturbed during HCS events.

We will compare the signatures associated with the sector boundary crossings found at the magnetotail of Venus with that is previously reported from comet studies.

References

[1] Edberg et al., 2011, Atmospheric erosion of Venus during stormy space weather, Journal of Geophysical Research, 116, A09308, doi:10.1029/2011JA016749

[2] Masunaga, K., Y. Futaana, M. Yamauchi, S. Barabash, T. L. Zhang, A. O. Fedorov, N. Terada, and S. Okano, O+ outflow channels around venus controlled by directions of the interplanetary magnetic field: Observations of high energy o+ ions around the terminator, J. Geophys. Res., 116(A9), doi: 10.1029/2011JA016705, 2011.

[3] Niedner, M. B and J. C. Brandt, 1978, Interplanetary gas. XXII—Plasma tail disconnection events in comets—Evidence for magnetic field line reconnection at interplanetary sector boundaries, Astrophys. J., 223, 655–670, doi:10.1086/156299.

[4] Zhang, T. L., J. Du, Y. J. Ma, H. Lammer, W. Baumjohann, C. Wang, and C. T. Russell, Disappearing induced magnetosphere at venus: Implications for close-in exoplanets, Geophys. Res. Lett., 36, doi: 10.1029/2009GL040515, 2009.

EPSC Abstracts
Vol. 10, EPSC2015-90, 2015
European Planetary Science Congress 2015

Validity of space weather prediction to Venus and Mars

A. Opitz (1), D. Vech (1, 2), E. Sanchez-Diaz (3, 4), K. Szego (1), O. Witasse (3), and N. Andre (4)
(1) Wigner Research Centre for Physics, Budapest, Hungary, (2) Lulea University of Technology, Kiruna, Sweden, (3) ESA / ESTEC, Noordwijk, Netherlands, (4) IRAP (CNRS-UPS), Toulouse, France (opitz.andrea@wigner.mta.hu)

Abstract

Both Venus and Mars have ionospheres, but no strong intrinsic magnetospheres, only Mars has some inhomogeneously distributed crustal field. The solar wind interaction with the ionosphere of these unmagnetized planets is highly important in defining the planets' plasma environment. The properties of their induced magnetospheres depend strongly on the solar input arriving at the planet. In order to study this interaction of the solar wind and the planetary plasma environment, ideally we would need measurements both in the solar wind and in this induced magnetosphere the same time. When there is only one spacecraft around the planet, it cannot perform such simultaneous observations, thus the prediction of solar wind properties and solar events to the different planetary objects becomes important. These predictions can be validated by in situ measurements onboard the planetary spacecraft such as Mars Express and Venus Express while these are located in the solar wind. The solar predictions are based on solar spacecraft observations such as SOHO, ACE, WIND, STEREO A and B, which are at different distances from the investigated planets. We show how the prediction accuracy depends on the spatial separation of the solar and the planetary spacecraft.

EPSC Abstracts
Vol. 10, EPSC2015-518, 2015
European Planetary Science Congress 2015

Hot Plasma Environment Model (HPEM): A empirical model for describing time-dependent processes of the jovian energetic electron environment

E. Roussos (1), N. Krupp (1), M. Fränz (1), P. Kollmann (2), P. Truscott (3) and Y. Futaana (4)
(1) Max Planck Institute for Solar System Research, Göttingen, Germany, (2) Applied Physics Laboratory, USA, (3) Kallisto Consultancy, UK, (4) IRF, Kiruna, Sweden (roussos@mps.mpg.de)

Abstract

HPEM is a model designed in order to provide time-series of energetic electron differential or integral energy-flux spectra for Jupiter's magnetosphere which can be used as input for internal charging studies of the JUICE spacecraft. The model describes the electron distribution function between 150 keV keV up to ~50 MeV. It is designed to be applicable between the orbit of Europa (9.5 Rj) up to 30 Rj, which is near Callisto's orbit, and in a latitude range of 40 degrees from the planetary equatorial plane, but it can be extended to larger distances and latitudes. The model is constructed with a goal to describe the time variability that a spacecraft can encounter in Jupiter's energetic electron environment. This variability can have two components: the first comes from the motion of the spacecraft within a spatially-varying jovian magnetosphere. For this purpose an average radiation belt model for the differential electron energy-flux spectra was constructed based on Galileo EPD/LEMMS observations, dependent on L, magnetospheric local time and equatorial pitch angle. The second component includes an empirical description of magnetospheric transients that result from dynamics in the magnetosphere. For this purpose, the probability for a given spectrum to deviate from the average one (at a given location) has been modeled with log-normal distributions and such probabilities are obtained with a Monte-Carlo approach. Temporal changes in the electron spectra are constrained by the L- or time gradients observed with Galileo's EPD/LEMMS detector so as to prevent extreme and unrealistic changes between sequential spectra of the model's output. The model is able to reproduce both the statistical scatter of energetic electron fluxes observed with Galileo/EPD, as well as the lifetimes/time scales and the occurence probability of extreme flux enhancements (temporal radiation belts) that Galileo encountered. An application to the JUICE mission is also shown.

EPSC Abstracts
Vol. 10, EPSC2015-599, 2015
European Planetary Science Congress 2015

Seasonal Variation of Martian Pick-up Ions

M. Yamauchi(1), T. Hara(2), R. Lundin(3), E. Dubinin(4), A. Fedorov(5), J.-A. Sauvaud(5), R.A. Frahm(6), R. Ramstad(1), Y. Futaana(1), M. Holmstrom(1), and S. Barabash(1)
(1) Swedish Institute of Space Physics (IRF), Kiruna, Sweden; (2) Space Sciences Laboratory, University of California, Berkeley, USA; (3) Swedish Institute of Space Physics (IRF), Umea, Sweden; (4) Max-Planck-Institut fur Sonnensystemforschung, Germany; (5) Institut de Recherche en Astrophysique et Planetologie (IRAP), CNRS/Universite de Toulouse, France; (6) Southwest Research Institute, 6220 Culebra Road, San Antonio, TX, 78238, USA

Abstract

Statistics of Mars Express (MEX) ion mass analyser (IMA) data shows that ion production from exospheric hydrogen depends more on the Sun-Mars distance than the solar cycle phase or winter-summer hemispheric difference. This indicates that the EUV is not the only driver of the production of cold, exospheric-origin ions, and that the extension of the exosphere is strongly influenced by total irradiance that carries the majority of the solar energy to the Martian atmosphere

1. Introduction

Mars Express (MEX) has operated for more than 10 years in the environment of Mars, providing solar wind ion observations by the Analyzer of Space Plasmas and Energetic Atoms (ASPERA-3) experiment's ion mass analyzer (IMA). In the region just outside the bow shock of Mars, IMA frequently observes ring-like distributed ions that include both pick-up ions of exospheric origin and reflected solar wind by the bow shock [1]. These observations have limitations on the detected angular distribution due to the limited field-of-view (FOV), on the low-energy proton detection due to sensor capability, and on the lack of the upstream magnetic field knowledge due to the absence of a magnetometer.

2. Analyses

Despite the lack of magnetic field data, the length and quality of the IMA data (nearly no degradation of the sensor efficiency) is sufficient to statistically diagnose the seasonal (defined by the Sun-Mars distance, and we call "summer" when the Mars is at perihelion) and solar cycle variation of the pick-up ions of exospheric origin. Two methods are employed for such statistical analyses: the automated method [2] and manual (eye-identified) method [3]. The automated method is used to obtain the general distribution whereas the manual method is used to obtain fine (2-months resolution) temporal variation, as shown in Figure 1. Both methods are applied to eight years of MEX/IMA data during 2005-2012.

3. Results

The statistics revealed that the occurrence rate of the pick-up ions varies with Sun-Mars distance, i.e., sharply increases during the Martian summer (Mars perihelion). This seasonal variation is dominant over the solar cycle variation that has a much longer time scale, and the occurrence probability is different for the same level of EUV flux, e.g., between the summer of the solar minimum and winter of solar maximum, results in different probabilities. The automated method further revealed that the variation is mainly driven by the Sun-Mars distance rather than the season of the (southern) hemisphere that possesses large magnetic anomalies. The temporal variation obtained by manual method also revealed that the peak occurrence rate is recorded slightly (1-2 month) after the perihelion.

4. Conclusion

The result indicates that the EUV is not the only driver of the production of cold, exospheric-origin ions, and that the extension of the exosphere is controlled more by the Sun-Mars distance than the EUV. One possibility is that the atmospheric condition (e.g., temperature or existence of dust) might strongly influence the exosphere.

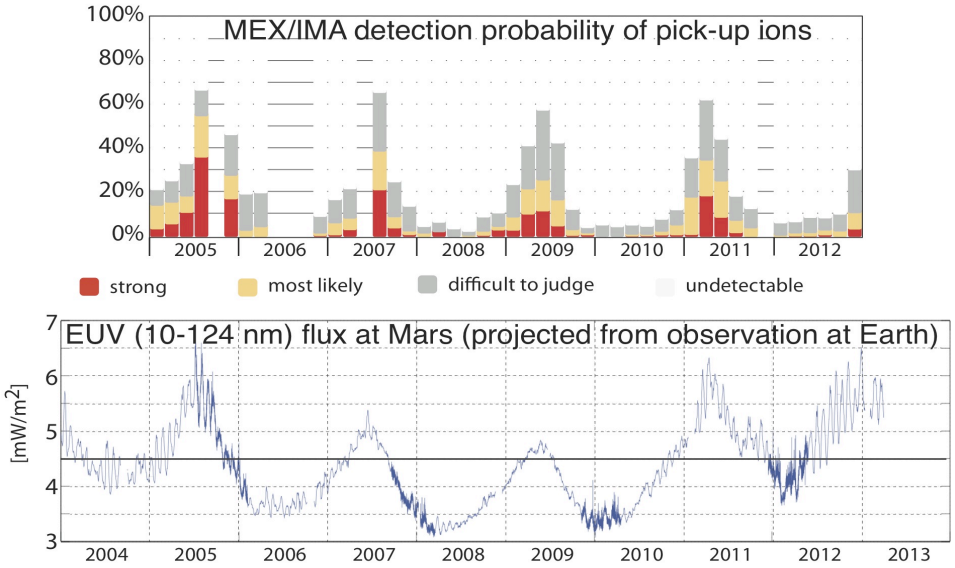

Figure 1: Temporal variation of (a) observation rate of the pick-up ions determined using the manual method, and (b) the estimated EUV flux at Mars from the measured value at the Earth by TIMED/SEE instrument [4]. There are about 7500 inbound or outbound traversals during 2005-2012 with the medium mass-resolution mode. Note that the total number of hours under a specific mass-resolution mode of IMA varies from time to time, and MEX is sometimes completely downstream of the bow shock for about one month. Therefore, taking monthly average is not appropriate. However, data becomes rather smooth if two months time intervals are integrated.

Acknowledgements

Both IMA and ELS are part of the ASPERA-3 experiment on the ESA Mars Express spacecraft. We are indebted to all of the involved national agencies and to the European Space Agency for conducting the Mars Express program, especially the Swedish National Space Board, CNRS in France, and NASA (contract NASW-00003) in the USA. EUV value at the Earth is provided by NASA's TIMED/SEE experiment. The sunspot numbers are provided by the Royal Observatory of Belgium, Brussels.

References

[1] Yamauchi, M., Futaana, Y., Fedorov, A., Dubinin, E., Lundin, R., Sauvaud, J.-A., Winningham, D., Frahm, R., Barabash, S., Holmström, M., Woch, J., Fraenz, M., Budnik, E., Borg, H., Sharber, J. R., Coates, A. J., Soobiah, Y., Koskinen, H., Kallio, E., Asamura, K., Hayakawa, H., Curtis, C., Hsieh, K. C., Sandel, B. R., Grande, M., Grigoriev, A., Wurz, P., Orsini, S., Brandt, P., McKenna-Lawler, S., Kozyra, J., and Luhmann, J. (2006): IMF direction derivation from cycloid-like ion distributions observed by Mars Express, Space Sci. Rev., 126(1-4), 239-266, doi:10.1007/s11214-006-9090-1

[2] Hara, T., Seki, K., Futaana, Y., Yamauchi, M., Barabash, S., Fedorov, A.O., Yagi, M., and Delcourt, D.C. (2013): Statistical properties of planetary heavy-ion precipitations toward the Martian ionosphere obtained from Mars Express, J. Geophys. Res. Space Physics, 118, 5348-5357 doi:10.1002/jgra.50494.

[3] Yamauchi, M., Futaana, Y., Fedorov, A., Frahm, R.A., Dubinin, E., Lundin, R., Sauvaud, J.-A., Winningham, J.D., Barabash, S., and Holmström, M. (2012): Ion acceleration by multiple reflections at Martian bow shock, Earth Planets Space, 64(2), 61-71, doi:10.5047/eps.2011.07.007.

[4] Woods, T. N., Eparvier, F. G., Bailey, S. M., Solomon, S. C., Rottman, G. J., Lawrence, G. M., Roble, R. G., White, O. R., Lean, J., and Tobiska, W. K. (1998): TIMED Solar EUV Experiment, SPIE Proceedings, 3442, 180-191.

EPSC Abstracts
Vol. 10, EPSC2015-781, 2015
European Planetary Science Congress 2015

The Filamentation of the TLE's

J. Błęcki (1), K. Mizerski (2), K. Słomińska (1), J. Słomiński (1) and S. Savin (3)

(1) Space Research Centre PAS, Warsaw, Poland, (2) Institute of Geophysics PAS, Warsaw, Poland, (3) Space Research Institute RAS, Moscow, Russia.

(jblecki@cbk.waw.pl / Fax: +48-22-8403131)

Abstract

The small scale structure of TLE's is discussed in the context of the filamentation processes. The discussion is focused around 3 mechanisms –pinch instability, filamentation of kinetic Alfven's waves and ionization instability.

1. Introduction

Plasma turbulence is one of the most significant features of the space plasma. Alfven, lower hybrid, electron and ion cyclotron waves and higher frequency waves at Langmuir and upper hybrid frequencies are always observed in the ionospheres, magnetospheres, solar wind.

Another general feature of a magnetized plasma is a tendency to create filamentary structures in the field aligned currents [1]. This filamentation can be seen by optical and X-ray observations of the solar chromosphere and corona, in the cometary's tails and on the Earth in the aurora. Magnetospheric plasma indicates also a tendency to form subtle structures in the current flowing along magnetic field line.

Prognoz-8, Magion-4, Interball Tail Probe and CLUSTER registered crossings of many small scale structures in different magnetospheric plasma domains. Examples of observation of these types of structures which we assumed are plasma filaments in the polar, magnetospheric cusp [2] are shown in Figures 1 and 2. The observed subtle structure of the TLE's indicate subtle structure which can be also identified with the plasma filaments.

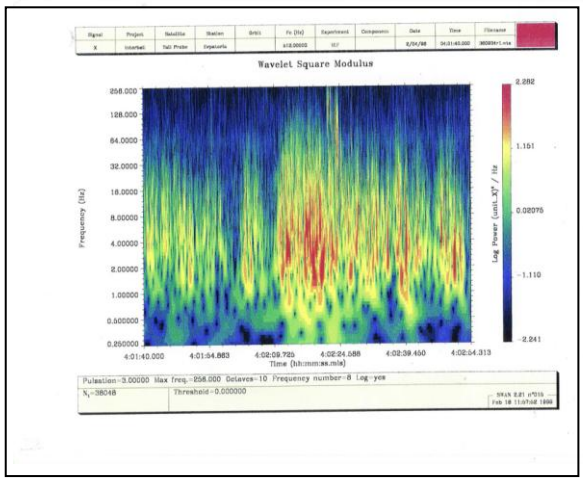

Figure 1: Wavelet spectra from Interball 1taken in the polar cusp. The variability of the wave intensity indicate crossing small scale structures within cusp.

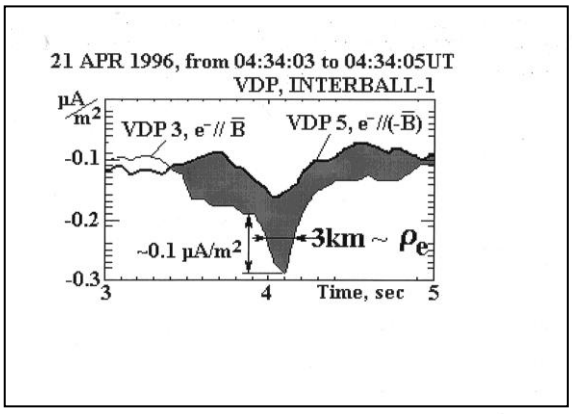

Figure 2: Filament of the electric current in the polar cusp registered by Interball 1 [2].

2. Transient Luminous Events (TLE's)

Transient Luminous Events (TLE) are upper atmospheric optical phenomena associated with thunderstorms. First suggestion on the existence of such phenomena was given by Scottish physicists C.T.R. Wilson in 1920's, but only 70 years later these phenomena were registered. The experimental discovery of these events was done accidentally in 1989 by Robert Franz . These first registrations were related to phenomenon which now is called red sprite [3],[4].

Since then thousands of observations of different types of TLEs have been done from the aircrafts, space shuttle, space station and satellites. The observations up to now are mainly related to optical phenomena. There are some different types of TLE- red sprites, blue jets, elves, halos and trolls. All of them are of the electromagnetic nature and are triggered by a rapid significant change in electric filed above the cloud level reaching to the ionosphere. The first proof that the electromagnetic effects observed in the mesosphere are generated by sprites and can be registered in the ionosphere has been done by DEMETER satellite observations [5] . These events are associated with the intense energy transfer between the atmospheric layers and have a strong influence on the ionosphere. Figure 3 presents the variety of the Transient Luminous Events.

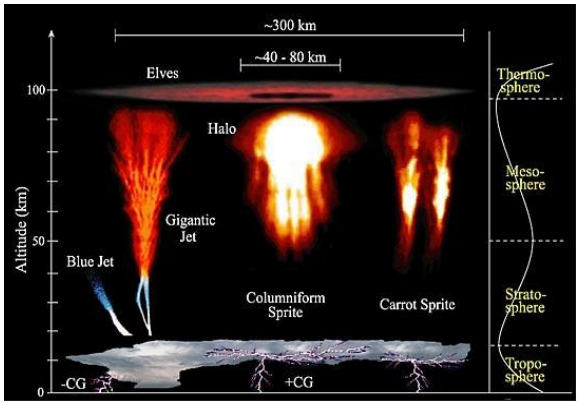

Figure 3: The view of the different phenomena called Transient Luminous Events

Sprites are associated with giant storm clouds with dimensions over 1000km producing strong electric field in the mesosphere. Sprites are massive but weak luminous flashes, appearing at altitudes 40-90 km.

Sprites are predominantly red. The brightest region lies in the altitude range 65-75 km, above which there is often a faint red glow structure that extends to about 90 km. Below the bright red region, blue tendril-like filamentary structures often extend downward to 40 km. Sprites rarely appear alone, they usually occur in groups - two, three or more

The duration of sprites is of the order of ms. Currents associated with sprites have intensity above 1 kA.

Blue jets are another high altitude optical phenomena, observed above strong thunderstorms. Blue jets are seen as an optical ejections from the top of the electrically most active regions of thunderstorms. Following their emergence from the top of the thundercloud, they typically propagate upward in narrow structure in form of cones of about 15 degrees full width at vertical speeds of roughly 100 km/s (Mach 300), fanning out and disappearing at heights of about 40-50 km. The giant blue jets can reach the ionospheric altitude . Their intensities are on the order of 800 kR near the base, decreasing to about 10 kR near the upper edge. These correspond to an estimated optical energy of about 4 kJ, a total energy of about 30 MJ, and an energy density on the order of a few mJ/m^3. Blue jets are rather rare events. Their appearance is much lower than sprites. Blue jets are not aligned with the local magnetic field.

The described above events are strongly electromagnetic events and its activity has direct influence on the conditions in the ionosphere.

3. Filamentary Structure of TLE's

Filamentary structures are found in the many cases of space plasmas, all of them are observed or are likely to be associated with electric currents: In the aurora filaments parallel to the magnetic field are often observed. These can have dimensions down to 100m; inverted V events (10^5 -10^6 A) and in situ measurements of the electric currents in the magnetosphere demonstrate the existence of the filamentary structures; in the ionosphere of Venus „flux ropes" or „magnetic ropes", whose filamentary diameter are typically 20km, are observed; on the Sun, prominences (10^{11}A), specula's, coronal streamers, polar plumes etc. show filamentary structure whose dimensions are in order 10^7-10^8m; the cometary tails often have a pronounced

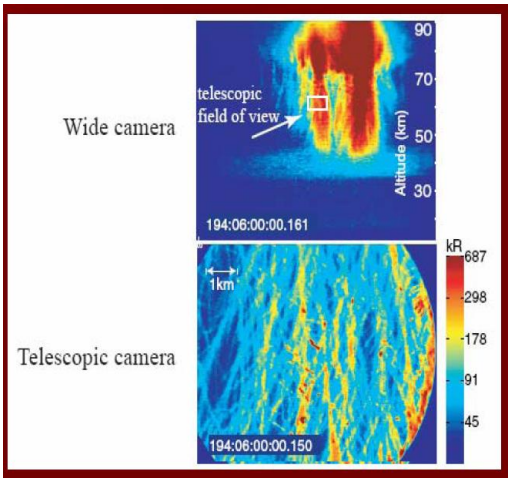

Figure 4: Subtle structure of the sprite [6]

filamentary structure, sprites and blue jets show the subtle structure along the current with spatial scales of the order tens to hundreds meters . Figure 4 shows the subtle structure of the sprite [6].

4. Physical Mechanisms of Filamentation

There are two fundamental physical mechanisms trying to explain a creation of the filamentary structure in the space plasmas. Both are associated with currents and ambient magnetic field.

1.Pinch instability of the field aligned electric current [7]. Galperin et al. suggested this mechanism as a source of the subtle structure of the aurora. Current layer is decomposed into small scale magnetic islands by this instability. The size of these islands is given by:

$$L \approx \frac{c}{\omega_p} \approx \frac{10^4}{\sqrt{n_e}}[m.]$$

The characteristic time of formation of these structures is given by:

$$\tau^* = 4\sqrt{\frac{m_i}{m_e}}\frac{m_e}{eB_{perp}}$$

2.Filament instability of the dispersive Alfven waves [8], [9], [10]. Magnetohydrodynamic description of the plasmas concentrates on length scales that are much longer than ion inertial length $L \approx \frac{c}{\omega_{pi}}$ and time scales much longer than inverse ion gyrofrequency Ω_i^{-1}.

The solution of these equations are dispersive Alfven waves. These waves are circular polarized and propagate along the magnetic field. Shukla and Stenflo find that transverse perturbation of these waves leads to formation of the paralell to the magnetic field alongated structures (filaments) due to so called filametation instability. The numerical simulation of the disturbances of the MHD Hall's equations done by Laveder et al. [8] fully confirm this result. The scheme of the physical mechanism of this instability is shown in Figure 5. The scale of generated structures can be determine by the local density as:

$$\lambda \geq \frac{2.2\times10^8}{n_e}[m.]$$

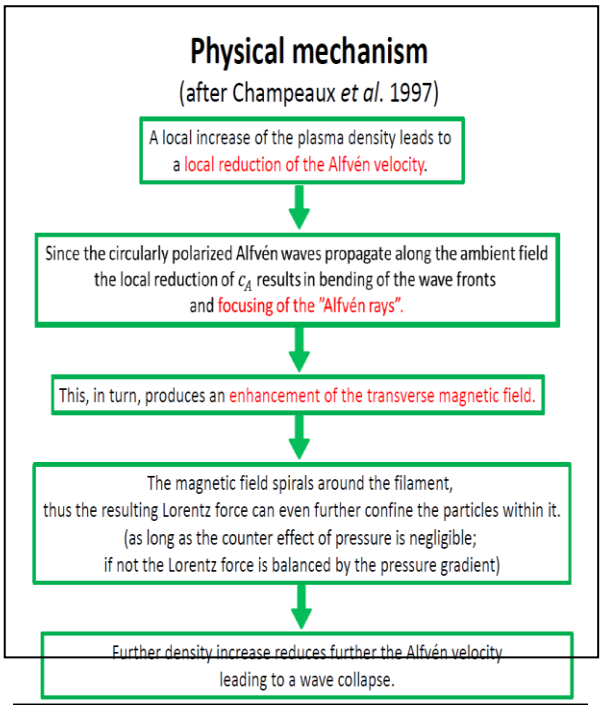

Figure 5: Physical mechanism of the filamentation instability.

5. Summary and Conclusions

The characteristic time scales of the fine structures in TLE correspond to characteristic time scales of TLE's and can be up to tens of miliseconds and the spatial scales are in order of tens to hundreds meters. The structures observed in the aurora have similar size ([7]and references given there).

The non-linear analysis of the kinetic Alfven waves shows the possibility of the filamentation of these waves with a minimum characteristic scale corresponding to characteristic scales of Alfven soliton [11]. The characteristic scale is of the order of the Alfven wave length. Its minimum value can be expressed by the local electron density: $\lambda_a \geq 2.2 \times 10^8 / n^{1/2}$[m] if the plasma density n is measured in m^{-3}.

Another non-linear mechanism which can lead to the filamentation is pinching of the field aligned electric current [7]. This mechanism can generate structures with a smallest size given by $L>c/\omega_p$ (c is the light velocity and ω_p the plasma frequency). It can be also expressed by the electron local density as $10^7/n^{1/2}$ [m].

Both characteristic scales depend strongly on the altitude. Assuming that proton density at the altitudes where TLE's appear 10^9-10^{10} m^{-3} what corresponds to Alfven wavelengths of 2.2-7 km and pinch generated structures of 100- 300 m. The application of these mechanisms to TLE's needs a further studies and we are currently doing that.

Another mechanism which is well known in laboratory plasmas and has been applied for explanation of the small scale irregularities of the electron concentration in the ionospheric electrojets (equatorial and auroral)- the ionization instability [12] can be also discussed as a source of subtle structure of TLE and we will discussed it in our further work.

Acknowledgements

This work has been supported by grant NCN 2014/13/B/ST10/01285

References

[1] Perrat A. L., Physics of the Plasma Universe, Springer Verlag, New York, Berlin, Heidelberg, London, Paris, Tokyo, Hong Kong, Barcelona, Budapest, 1991.

[2] Błęcki J., Savin S., Cornilleau-Wehrlin N., Kossacki K., Parrot M., Nemecek Z., Safrankova J., Wronowski R., Kudela K., Santolik O.. The Low Frequency Plasma Waves in the Outer Polar Cusp – Review of Observations from Prognoz 8, Magion 4, INTERBALL 1 and CLUSTER Satellites, Survey in Geophysics,.vol. 26. Nr 1-3 pp177-191, 2005

[3] Sprites, Elves and Intense Lightning Discharges, eds. Fullekrug M., Mareev E., Rycroft M., Springer, Heidelberg, 2006.

[4] Torsten Neubert, On Sprites and Their Exotic Kin, Science ,vol. 300, 2 May 2003

[5] J. Błęcki , M. Parrot, R. Wronowski, ELF and VLF signatures of sprites registered onboard the low altitude satellite DEMETER, Annales Geophysicae, 27, 2599–2605, 2009

[6] Gerken, E. A., Inan, U. S., and Barrington-Leigh, C. P. Telescopic imaging of sprites. Geophys. Res. Lett., 27:2637–2640, 2000.

[7] Galperin Yu., Zelenyi L., Kuznetsova M., Pinching of the Field – Aligned Currents as a Possible Mechanism of the Aurora Ray Structures Formation, Cosm. Res., XXIV, pp. 865-874, 1986.

[8] Laveder D., Passot T., and Sulem P.L., Instabilities and Filamentation of Dispersive Alfven Waves, World Scientific, 2001.

[9] Shukla P. K. and Stenflo L., Filamentation Instability of the Dispersive Plasma Waves, Space Science, 1989.

[10] Champeaux S., Gazol A., Passot T., and Sulem P.L, Plasma Heating by Alfven Wave Filamentation: A Relevant Mechanism in the Solar Corona and the Interstellar Medium The Astrophysical Journal, 486:477-483, 1997.

[11] Bingham R., Bryant, D. A., and Hall, D. S., Auroral Particle Acceleration by Waves, Phys. Chem. Earth, **26**, 133-144, 2001.

[12] Błęcki J., Ionisation Instability as a Source of Electron Density Irregularities in the Equatorial electrojet, Publs. Inst. Geoph. E-1 (100),1976.

EPSC Abstracts
Vol. 10, EPSC2015-815, 2015
European Planetary Science Congress 2015

THEMIS Na exosphere observations of Mercury and their correlation with *in-situ* magnetic field measurements by MESSENGER

V. Mangano (1), S. Massetti (1), A. Milillo (1) , C. Plainaki (1), S. Orsini (1), R. Rispoli (1) and F. Leblanc (2)

(1) INAF/IAPS, Roma, Italy (2) LATMOS/IPSL, Paris, France
(valeria.mangano@iaps.inaf.it)

Abstract

The Na exosphere of Mercury is being studied since its discovery in mid '80s from Earth-based telescopes, and it has revealed a high dynamics and variability. Although the processes and their relationships characterising the Hermean exosphere generation and dynamics are still not exhaustively understood, there are no doubts on a tight interconnection among the planet's surface, exosphere, intrinsic magnetic field, the Solar Wind and the Interplanetary Magnetic Field (IMF). Here we analyse an extended dataset of images of the exospheric Na emission, collected from 2009 to 2013, by means of the THEMIS ground-based telescope, and perform a comprehensive statistical study of the recurrent Na emission patterns, and also their potential relationship with the IMF variability. For this purpose, we take advantage of a subset (years 2011-2013) of contemporary *in situ* measurements of the IMF obtained by the MAG instrument on-board the MESSENGER spacecraft.

1. THEMIS data:recurrent patterns

A wide database of 644 images obtained from yearly observations of Mercury by the THEMIS solar telescope in Tenerife is analyzed to identify the recurrent Na emission patterns for years 2009-2013. They can be mainly divided into two categories: single peak centered on the sub-solar point, or two symmetric peaks at high/mid latitude position along noon meridian. Inside each of the two categories, we can further divide the different morphologies into 8 different types (see Figure 1). Final unbiased statistical analysis of the 377 'good' images are summarized in Table 1 where the images are also divided according to the geometry of observation (East or West longitude). Table 1 shows that the symmetrical (with respect to equator) single peak pattern EP (9.3%) and unsymmetrical single peak patterns EPN (6.9%) and EPS (6.1%) occur in 84 cases (22.3%). The WP is about twice as frequent as EP (16.4%). The remaining 61.3% of cases belongs to double peaks patterns: 45 cases of 2P (11.9%), 45 of 2PC (11.9%), 80 cases of 2PN (21.2%) and 61 of 2PS (16.2%). These data confirms that, on the long term, the double peak emission is the most frequent Na exospheric configuration. On the other hand, the most frequent exospheric Na emission pattern is a different one each year, that is: 2P in 2009, 2PS in 2010, 2PN in 2012 and in 2013. The 2011 only shows a predominance of the single peak patterns (EP and WP).

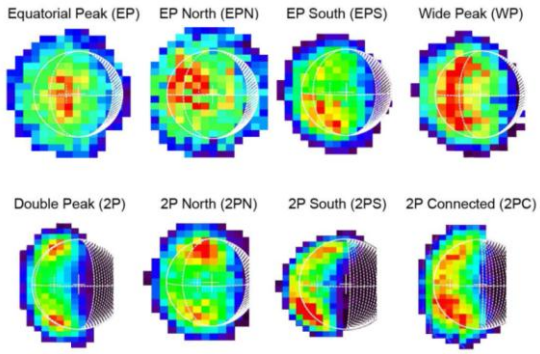

Figure 1: The 8 recurrent Na emission patterns.

Table 1: List of the 8 different exospheric patterns.

TYPE OF PATTERN	2009			2010			2011			2012			2013			5 years			total
	east	west	tot	east	west	tot	east	west	tot	east	west	tot	east	west	tot	east	west	tot	
Equatorial peak		7	7		4	4	12	10	22	1		1	1		1	14	21	35	
E. Peak North				2		2		3	3	15		15	6		6	23	3	26	84
E. Peak South		6	6		12	12		4	4					1	1		23	23	
Wide peak		7	7	7	5	12	1	26	27	9		9	7		7	24	38	62	62
2 Peaks	25	8	33		3	3		2	2	5		5	2		2	32	13	45	
2 Peaks Connected	3	7	10	3	7	10		5	5	15		15	5		5	26	19	45	231
2 Peaks North +	27	1	28	2	4	6		2	2	30		30	14		14	73	7	80	
2 Peaks South +	4	11	15		32	32		7	7	1		1	1	5	6	6	55	61	
TOTAL			106			81			72			76			42			377	
																			644
Rejected			82			49			29			13			94			267	

2. THEMIS data: full-disk analysis

In addition, we use a subset of images (79) taken when most of the illuminated disk was in view (≥ 90%) to account for the possible reasons of these symmetries, and to analyse whether asymmetries occur also in longitude. A summary is given in Table 2. We analysed the position of the Na emission patterns (both single and double peak) with respect to the sub-solar meridian (noon) and subdivided them into three regions: *pre-noon*, *noon* and *post-noon*, accordingly to the location of the patterns (see Figure 2), and found that they are mostly located in the pre-noon (53%) and noon (35%) regions (see Table 2). A check on the East or West elongation occurring during the observation shows that the subset of images is equally distributed between Eastern and Western elongations, hence minimizing possible systematic errors due to visual geometry. In addition, we also find that the Double Peak patterns observed in this set of *quasi-full disk* images are all roughly located along the same meridian, i.e. no longitudinal shift of one peak with respect to the other is clearly evidenced.

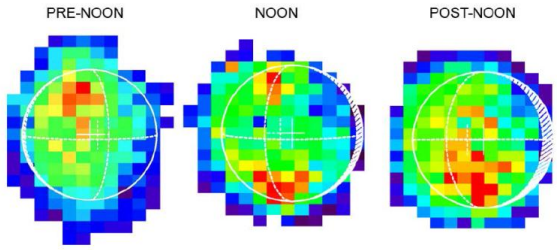

Figure 2: Examples of the pre-noon, noon and post-noon Na emission patterns.

Table 2: List of the 8 different exospheric patterns in the sub-set of 90% visibility of the disk.

TYPE OF PATTERN	2009			2011			2012			2013			5 years			Total
	pre	noon	post	pre	noon	post	pre	noon	post	pre	noon	post	pre	noon	post	
Equatorial peak	3	2					1						4	2		
E. Peak North					2	1	11				1		11	3	1	27
E. Peak South	4	1										1	4	1	1	
Wide peak	4	1				2	3	1					7	2	2	11
2 Peaks		1			1			1						3		
2 Peaks Connected	5				2		4	1	1				9	3	1	41
2 Peaks North +						1	2	5	2	1		2	3	5	5	
2 Peaks South +	3	4								1	4		4	8		
TOTAL	19	9	0	0	5	4	21	8	3	2	5	3	42	28	9	79

3. MAG data & correlation with THEMIS

Depending on the spacecraft position along the orbit, the MAG sensor collects data from both the IMF or the magnetosphere of Mercury (Figure 3). MESSENGER was orbiting around Mercury since March 2011. Hence, since that moment contemporary data of global exospheric Na mapping and in-situ measurements of the IMF B-field are available (years 2011-2013). We calculated the occurrence of the different patterns for each IMF component, by subdividing the magnetic field strength and sign into four ranges: $B_i \geq 10$ nT, 10 nT $\geq B_i \geq 0$ (strongly and moderately positive), $0 \geq B_i \geq -10$ nT , -10 nT $\geq B_i$ (moderately and strongly negative). Table 3 summarizes the results (NB. Note that we have only 1 2PS event occurring in the present analysis and it was omitted from the statistics).The stronger correlation between IMF and Na emission patterns occurs for the double peak set, where IMF B_x is mainly > 0, and IMF B_y < 0. The IMF B_z is strongly negative in the 2P case. On the contrary, the single peak set shows less definite correlation: IMF B_x ranges from strongly positive to strongly negative, in EP and WP configurations, respectively. The IMF B_z is mostly negative in EP patterns (58%), while is positive in 53% of WP ones.

SINGLE PEAK

	Bx	By	Bz	Bx	By	Bz	
B ≥ 10	39%	34%	9%	37%	37%	14%	ALL
0 < B < 10	6%	30%	40%	3%	23%	40%	
-10 < B < 0	6%	21%	36%	11%	20%	23%	
B ≤ -10	49%	15%	15%	49%	20%	23%	
B ≥ 10	75%	8%	17%	67%	13%	21%	EP
0 < B < 10	8%	25%	25%	0%	27%	53%	
-10 < B < 0	0%	42%	50%	6%	33%	13%	
B ≤ -10	17%	25%	8%	27%	27%	13%	
B ≥ 10	21%	42%	0%	17%	50%	11%	WP
0 < B < 10	5%	37%	53%	5%	22%	33%	
-10 < B < 0	5%	10%	31%	17%	11%	28%	
B ≤ -10	69%	11%	16%	61%	17%	28%	
	THEMIS – MAG (-1 h)			THEMIS – MAG			

≥ 70%
≥ 50%
≥ 33%
≥ 25%
≥ 20%
0-19

DOUBLE PEAK

	Bx	By	Bz	Bx	By	Bz	
B ≥ 10	71%	17%	12%	70%	19%	16%	ALL
0 < B < 10	0%	17%	37%	0%	21%	33%	
-10 < B < 0	3%	20%	37%	2%	9%	35%	
B ≤ -10	26%	46%	14%	28%	51%	16%	
B ≥ 10	72%	14%	13%	88%	13%	12%	2P
0 < B < 10	0%	29%	29%	0%	12%	12%	
-10 < B < 0	14%	14%	29%	0%	12%	13%	
B ≤ -10	14%	43%	29%	12%	63%	63%	
B ≥ 10	73%	18%	19%	57%	29%	14%	2PC
0 < B < 10	0%	19%	27%	0%	21%	36%	
-10 < B < 0	0%	27%	27%	0%	7%	43%	
B ≤ -10	27%	36%	27%	43%	43%	7%	
B ≥ 10	69%	19%	6%	70%	15%	15%	2PN
0 < B < 10	0%	12%	50%	0%	25%	40%	
-10 < B < 0	0%	13%	44%	5%	10%	40%	
B ≤ -10	31%	56%	0%	25%	50%	5%	
	THEMIS – MAG (-1 h)			THEMIS – MAG			

Table 3: Statistics of the IMF B_X , B_Y and B_Z 1-h averages. On the top/bottom the results obtained in the case of for the single/double peak patterns. The right columns show the IMF averages computed on the same time period of the Na measurements (THEMIS-MAG), the left ones show the IMF averages calculated 1-hour ahead the observations (THEMIS-MAG (-1 h)). Darker cells and bold digits indicate higher occurrence rates (see legend). Cells marked with thick borders indicate the most significant IMF B_Z values.

4. Conclusions

We performed a statistical analysis of the Na emission from the exosphere of Mercury, based on ground based observations taken by the THEMIS telescope, and spanning over a time period of 5 years (2009-2013). We categorized the exospheric Na emission into 8 different recurrent patters and studied their occurrence rate, also as a function of the in situ IMF, as measured by the MAG instrument on-board the MESSENGER spacecraft. The results of this study can be summarized as follows:

1. by considering the whole THEMIS database, we found that the equatorial peak patterns and the high latitude double peak patterns are mutually exclusive. The latter being the most common (61%) Na emission feature, often observed continuously for several hours: this supports the idea that the solar wind ion precipitation through the polar cusps has a crucial role in the generation of the observed high latitude Na exospheric emission;

2. on average, the observed double peak patterns do not show a statistically significant North-South asymmetry: if these are actually connected to the ion precipitation into the polar cusps, this fact favours the idea that the Mercury's magnetic dipole is symmetrical with respect to the equatorial plane, and also implies that the role of the IMF B_X in driving the magnetic reconnection in the Hermean magnetosphere is weaker than foreseen;

3. the analysis of the exospheric Na emission pattern as a function of the IMF, even if preliminary (due to the difficulty to have simultaneous in-situ IMF data), shows that the high latitude double peak pattern (2P) is more frequently observed during negative IMF B_Z periods (76%), whereas the single equatorial peak emission (EP) is more common when the IMF B_Z is positive (74%);

4. there exists a noticeable annual North-South asymmetry that, on the base of the present data, may be connected to a long-term external cause (e.g. the IMF variability in the inner heliosphere);

5. the analysis of the subset of quasi-full disk images shows that the Double Peak emission patterns are typically aligned in longitude, without any appreciable longitudinal shift possibly produced by a strong IMF $B_Y \neq 0$. It also shows that the Na emission is mostly located in the pre-noon sector (53%), which is roughly facing the local Parker's spiral direction, and close to the noon meridian (36%).

EPSC Abstracts
Vol. 10, EPSC2015-822, 2015
European Planetary Science Congress 2015

Space weather phenomena at Galilean moons and comets (invited)

G. Cessateur (1), M. Barthelemy (2), J. De Keyser (1), F. Dhooghe (1), J. Loreau (3), R. Maggiolo (1), A. Gibbons (1,3), N . Vaeck (3), K. Altwegg (4,5), L. Le Roy (5), J.-J. Berthelier (6), U. Calmonte (4), S. A. Fuselier (7), M. Hässig (8), M. Rubin (5), T. I. Gombosi (9) and M. Combi (9).

(1) Space Physics division, Belgian Institute for Aeronomy, Brussels, Belgium,(2) Institut de Planétologie et d'Astrophysique de Grenoble, Université Joseph Fourier, Grenoble, France, (3) Quantum Chemistry and Photophysics Laboratory, Université Libre de Bruxelles, Brussels, Belgium, (4) Physikalisches Institut, University of Bern, Sidlerstr. 5, CH-3012 Bern, Switzerland, (5) Center for Space and Habitability, University of Bern, Sidlerstr. 5, CH-3012 Bern, Switzerland, (6) LATMOS/IPSL-CNRS-UPMC-UVSQ, 4 Avenue de Neptune F-94100, Saint-Maur, France, (7) Department of Space Science, Southwest Research Institute, 6220 Culebra Rd., San Antonio, TX 78228, USA, (8) Max-Planck-Institut für Sonnensystemforschung, Justus-von-Liebig-Weg 3, 37077 Göttingen, Germany, (9) Department of Atmospheric, Oceanic and Space Sciences, University of Michigan, 2455 Hayward, Ann Arbor, MI 48109, USA.

Abstract

The exploration of planetary environments other than Earth has led to the definition of planetary space weather. We will mainly focus on the impact of the solar UV radiation which is responsible for the photoionization and photodissociation processes within planetary and cometary atmospheres. Those studies are of primary importance especially in the framework of the JUICE and ROSETTA missions.

A 1-D model has been developed in order to infer airglow emissions from Europa and Ganymede, from neutral atmospheric models. Considering various production and loss mechanisms, we estimate red and green line emission for atomic oxygen. The impact of precipitating particles has also been studied in order to estimate auroral emission, for the oxygen lines at 130.5 and 135.5 nm using radiative transfer modelling. Comparison with observations such as in situ measurements from Galileo, or remote observations from the Hubble Space Telescope, shows a good agreement that ensures us to provide reasonable constraints for the JUICE mission.

Modelling of the impact of the solar UV flux has also been done regarding cometary atmospheres, using in-situ measurement from the DFMS/ROSINA spectrometer onboard the ROSETTA spacecraft. Airglow emissions for the red line at 630 nm have then been estimated, considering various volatiles within the coma such as water, CO, and CO_2.

EPSC Abstracts
Vol. 10, EPSC2015-894, 2015
European Planetary Science Congress 2015

Low-coronal Sources of Stealth CMEs

N. Alzate and H. Morgan
Institute of Mathematics, Physics and Computer Science, Aberystwyth, Cymru (naa19@aber.ac.uk)

Abstract

Coronal mass ejections (CMEs) usually exhibit lower-corona dynamics such as flares, magnetic reconfiguration, EUV waves, jets or filaments. Recent studies have observed CMEs without a low-coronal signatures (LCS) which have been referred to as stealth CMEs. Through new image processing applied to EUV images we find clear evidence of LCS leading to stealth CMEs. The LCS of stealth CMEs are fairly sizeable yet faint eruptions with structure consistent with a rising flux tube, possibly formed higher in the corona in regions of weaker magnetic field. We believe these flux tubes are formed mostly in polar regions due to the large shear resulting from the slowly-rotating lower atmosphere below the more rapidly rotating corona. This would allow the formation of large flux tubes in weaker field regions, leading to low-energy and low-density flux tube eruptions.

1. Introduction

Coronal mass ejections (CMEs) are eruptions in the solar atmosphere which expand and propagate from the low corona to the interplanetary space [e.g. 1]. They are generally associated with eruptive phenomena in the lower corona such as solar flares, filament eruptions, EUV waves or jets, known as LCS.

[2] describe an event where there was no clear indication of a filament eruption or flare prior to a CME observed by white light coronagraphs. The lower coronal event leading to this stealth CME originated in a streamer at relatively large height. They interpreted this event as a very slow-rising flux tube leading to a streamer blowout CME. More recent work assembled a catalogue of ~40 stealth CMEs over a period of one year (2012), showing them to be relatively frequent events and revealing their unexplained preponderance over the North polar region [3]. The observational and kinematic properties of the 40 stealth CMEs were analyzed and compared to those of regular CMEs. To classify the events in the study, they searched for flares, filaments, EUV waves, jets, coronal dimmings, reconfiguration of the magnetic field in the higher corona, and flows in CACTus LASCO data coupled with the GOES/XRS data and the SoFAST catalog. Through visual inspection of SWAP, SDO and STEREO data, they narrowed down their data set to ~40 stealth CMEs.

As research suggests, the interaction between solar eruptions and the solar wind can create phenomena in the solar corona which are observed daily by space-based instruments. New image processing techniques can be applied to EUV [4] and white light coronagraph data [5] to reveal new detail. In this work, the new processing methods are applied to some of the data identified to contain stealth CMEs by [3] to investigate the possible existence of observable LCS.

2. Observations and methods

The instruments used in this study are the Large Angle and Spectrometric Coronagraph (LASCO) C2 which makes white light coronagraph observations, the Solar Dynamics Observatory (SDO)/Atmospheric Imaging Assembly (AIA) which images the solar atmosphere in seven extreme ultraviolet channels and three ultraviolet visible channels, and the Extreme Ultra-Violet Imager (EUVI) aboard the Solar Terrestrial Relations Observatory (STEREO).

LASCO C2 images were processed using the dynamic separation technique [4] and SDO/AIA and STEREO/EUVI images were processed with the new Multiscale Gaussian Normalization technique [5]. The method reveals fine details in the corona and can also reveal structure in off-limb regions.

3. Results

[3] identified 40 CMEs without low-coronal signatures occurring in 2012. One of these events took place on 23 February. Using our image processing techniques, we processed EUV data for this and similar events and compared results. Figure 1 is a composite image of this event in LASCO C2

and SDO/AIA 171. In the SDO image, we see activity in the lower corona we believe is evidence of LCS leading to the stealth CME identified in LASCO C2. Like this, we find other signatures in the lower corona, closer to the sun's surface, that may have caused the CME initiation process. This is shown in Figure 2. The same approach will be taken to study other cases listed in [3].

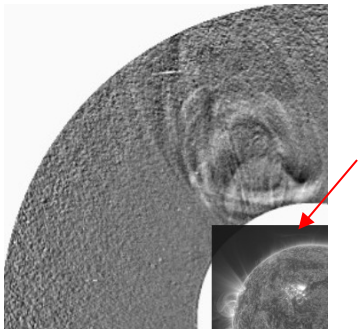

Figure 1: Outer: A CME seen in LASCO C2 data. Inner: Same event seen in SDO/AIA after our processing in which a low-coronal signature is visible (indicated by arrow).

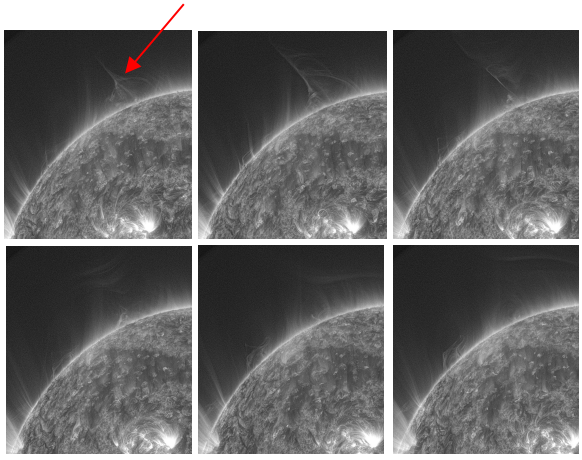

Figure 2: Coronal signatures (marked by arrow in first frame) associated with a stealth CME.

4. Discussion

- We are in agreement with conclusions of [2] and [3] that LCS of stealth CMEs are very faint events which form higher in the corona or in low-density regions of magnetic field weaker than usual CME-forming regions (i.e. filament eruptions or active regions).

- The 23 February 2012 event has the appearance of a large flux tube which through reconnection erupts slowly. It has low energy and very low initial velocity and acceleration.

- The differential rotation of the photosphere and the fact that the corona is a rigid rotator compared to the underlying photosphere [6] causes the formation at high latitudes. We believe this can lead to formation of large flux tubes following mechanisms similar to those described in [7], but in regions of weaker field and low density.

- We cannot explain the preference for formation of stealth CMEs in the North, but this is possibly due to the size and shape of the polar coronal hole.

5. Summary

Through careful processing of EUV images, we are able to show low-coronal signatures which lead to ejections previously referred to as stealth CMEs. With height-time profiles, we are able to show low-coronal events that appear to line up with stealth events. Proper fitting of these curves and further analysis will be able to confirm this.

References

[1] Chen, P. F.: Coronal Mass Ejections: Models and Their Observational Basis, LRSP, Vol. 8, 1, 2011

[2] Robbrecht, E., Patsourakos, S. & Vourlidas, A.: No Trace Left Behind: STEREO Observation of a Coronal Mass Ejection Without Low Coronal Signatures, ApJ, Vol. 701, 283, 2009

[3] D'Huys, E., Seaton, D. B., Poedts, S. & Berghmans, D.: Observational Characteristics of Coronal Mass Ejections Without Low-Coronal Signatures, ApJ, Vol. 795, 49, 2014

[4] Morgan, H., Byrne, J. P., & Habbal, S. R.: Automatically Detecting and Tracking Coronal Mass Ejections. I. Separation of Dynamic and Quiescent Components in Coronagraph Images, ApJ, Vol. 752, 144, 2012

[5] Morgan, H. & Druckmuller, M.: Multi-Scale Gaussian Normalization for Solar Image Processing, SoPh, Vol. 289, 2945, 2014

[6] Morgan, H.: The Rotation of the While Light Solar Corona at Height 4 Rs From 1996 to 2010: A Tomographical Study of Large Angle and Spectrometric Coronagraph C2 Observations, ApJ, Vol. 738, 189

[7] Ballegooijen, A. A. & Martens, P. C. H.: Formation And Eruption of Solar Prominences, ApJ, Vol. 343, 971, 1989

EPSC Abstracts
Vol. 10, EPSC2015-935, 2015
European Planetary Science Congress 2015

The COSPAR space weather road map

M. Grande and the COSPAR space weather team
(1) University of Aberystwyth, Institute of Mathematical and Physical Sciences, United Kingdom (mng@aber.ac.uk)

Abstract

Will be submitted later.